IEEE Photonics Journal
An IEEE Photonics Society Publication

Open Access

Acceleration of Carrier Lifetime in Gain-Clamped Semiconductor Optical Amplifiers

Volume 10, Number 5, September 2018

O. M. Kharraz
A. S. M. Supa'at
A. F. Abas
M. T. Alresheedi
M. A. Mahdi

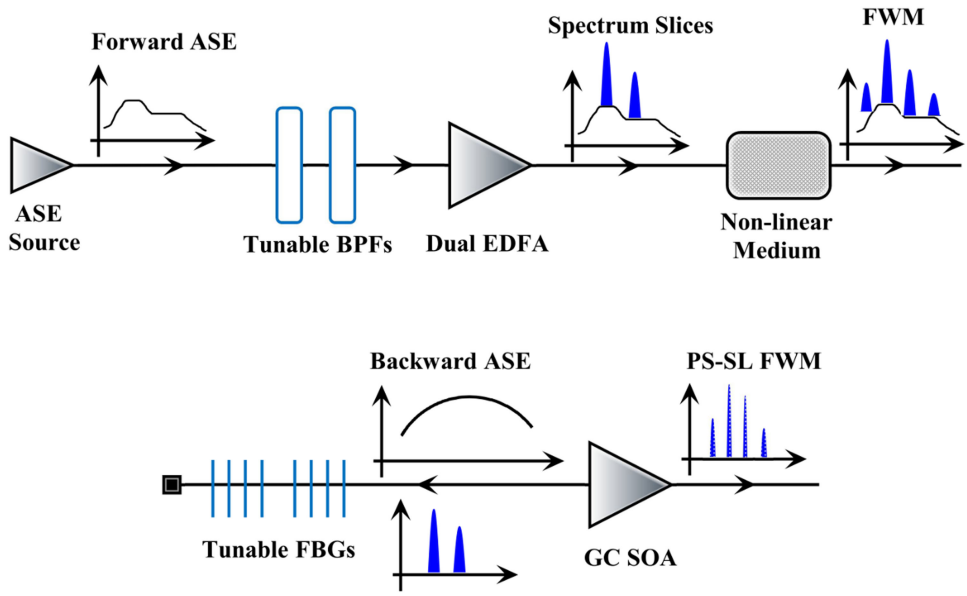

DOI: 10.1109/JPHOT.2018.2863254
1943-0655 © 2018 IEEE

Acceleration of Carrier Lifetime in Gain-Clamped Semiconductor Optical Amplifiers

O. M. Kharraz,[1] A. S. M. Supa'at,[1] A. F. Abas,[2] M. T. Alresheedi,[2] and M. A. Mahdi [3]

[1]Departement of Communication Engineering, Faculty of Electrical Engineering, Universiti Teknologi Malaysia, Skudai 81310, Malaysia
[2]Department of Electrical Engineering, College of Engineering, King Saud University, Riyadh 11421, Saudi Arabia
[3]Wireless and Photonics Networks Research Centre, Faculty of Engineering, Universiti Putra Malaysia, Serdang 43400, Malaysia

DOI:10.1109/JPHOT.2018.2863254

Manuscript received June 26, 2018; revised July 26, 2018; accepted July 31, 2018. Date of publication August 6, 2018; date of current version August 22, 2018. This work was supported by the International Scientific Partnership Program ISPP at King Saud University through ISPP#0106. Corresponding author: Osayd M. Kharraz (email: osayd-pd@utm.my).

Abstract: A new method to accelerate the carrier lifetime in semiconductor optical amplifiers (SOAs) is experimentally demonstrated. The four-wave mixing (FWM) effect is induced without recourse to external optical light sources. A pair of fiber Bragg gratings is utilized to generate pre-spectral sliced seed light channels as FWM inputs, by reflecting the backward amplified spontaneous emission from the SOA in a gain-clamped configuration. The theory predicts a three times shorter carrier lifetime, compared to coherent inputs in a travelling-wave arrangement. Furthermore, this method can be a more accurate measure of the nonlinear parameters of SOAs rather than conventional techniques, owing to the polarization-independent nature of the corresponding incoherent products.

Index Terms: Semiconductor optical amplifier (SOAs), carrier lifetime, gain-clamping, four-wave mixing.

1. Introduction

Semiconductor optical amplifiers (SOAs) for high-speed all-optical signal processing are still showing great promise, due to their inherently highly non-linear properties. An example of this, is a refractive non-linearity a hundred times greater than that of an equivalent length of optical fiber [1]. However, next generations of multi-functional processing applications require SOAs to possess faster gain recovery to cope with pattern effects, and to consequently operate at high-speed bit rates. The response of conventional bulk and quantum-well (QW) SOAs is still currently tied up by their long carrier lifetimes - of the order of hundreds of picoseconds [2]. In order to speed up the carrier lifetime of SOAs, many approaches have been reported in the literature. One method proposed the use of an external holding beam at a transparency point [2]–[5]. However, the injection of continuous-wave assisted light only increases complexity, and requires very large input optical powers. The gain of the SOA is then considerably reduced and, furthermore, this causes spectral broadening and distortion. Another approach has involved the use of quantum-dot (QD) and doped QW SOAs [6]–[8]. Additional methods have also incorporated a custom-made

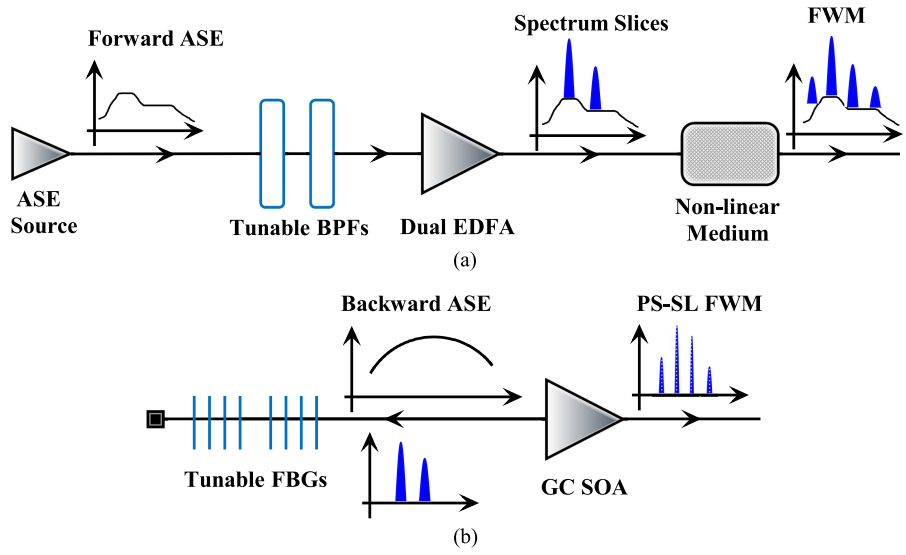

Fig. 1. Operation principle of (a) conventional SS-SL FWM technique based TW-SOA arrangement and (b) PS-SL FWM technique based GC-SOA configuration.

SOA, designed carefully with high amplified spontaneous emission (ASE) [9]–[11]. This approach involved the use of SOAs operating at high driving currents, which may not be commercially viable.

The carrier lifetime of SOAs is inversely proportional to saturation intensity of light, in which, efficient saturations occurring in gain media lead to higher stimulated recombination rates. The pre-spectrum sliced seed light (PS-SL) technique has been introduced to improve the power efficiency of the conventional spectrum-slicing seed light (SS-SL) technique [12], [13] and to also enhance the modulation bandwidths of amplifiers [14]. The PS-SL technique leads to efficient saturation occurring in gain-clamped (GC) configurations. The backward ASE of an erbium-doped fiber amplifier (EDFA) is spectrally sliced by a wavelength division multiplexer, and then reflected back by optical mirrors and re-injected into the EDFA. PS-SL re-injection of spectrum-sliced channels permits better energy and cost efficiency than that provided by the necessary multiple amplification procedures accompanied with other SS-SL techniques. Fig. 1 (a) shows the operational principle of four-wave mixing (FWM) based on the SS-SL technique in a travelling-wave (TW) SOA. An incoherent broadband light source, such as ASE, is spectrally sliced by means of tunable and multiple band-pass filters. The operational principle of FWM based on PS-SL proposal in a GC SOA is illustrated in Fig. 1 (b). The generated PS-SL channels are trimmed, pure and amplified - compared to original spectrum-sliced inputs due to the interactions between the backward ASE and PS-SL components at the input of SOA. The SOA is employed as a common ASE source, a GC amplifier and a non-linear medium concurrently.

In this work, we present a simple technique to accelerate the carrier lifetime of a SOA, via its backward ASE in a GC arrangement. PS-SL inputs are used to induce a FWM effect, in order to characterize the non-linear parameters of SOA under-test. This approach requires neither tunable RF nor laser sources, but the backward ASE of the employed bulk SOA is exploited efficiently without recourse to any active devices. Section 2 details the theoretical background. The characterizations of the SOA and the experimental set-ups used are then described in Section 3. The results and discussions are subsequently explained and analyzed in Section 4. Finally conclusions are given in Section 5.

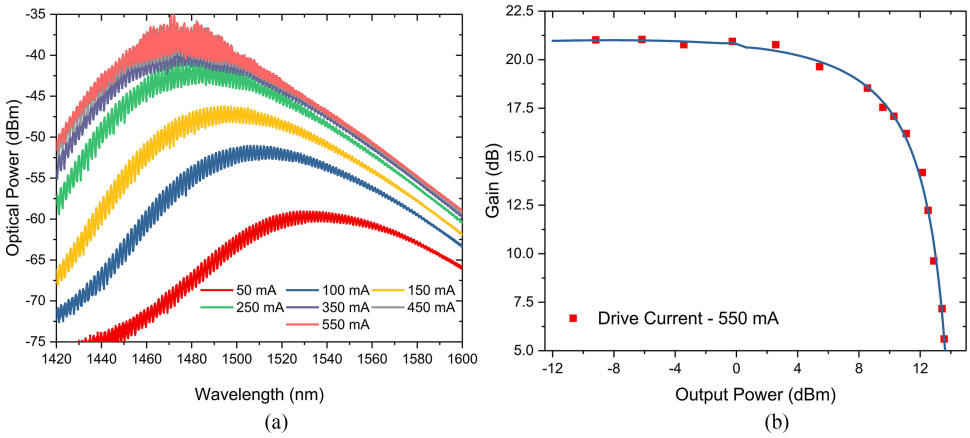

Fig. 2. (a) Measured ASE spectra at different operational currents (OSA resolution: 0.02 nm). (b) Output power versus gain responses with SOA bias current at 550 mA.

2. Theoretical Background

The analytical model presented in [15] is used to extract the non-linear fitting parameters of the SOA employed in the experiment. The saturation processes and propagation effects of the SOA are taken into account, thus classifying this model as a persuasive tool for analyses of FWM. An understanding of the theory that forms the basis for this model is useful for determining the related values of merit, such as conversion efficiency, for given device parameters. This understanding is therefore valuable when applying the model to extract the SOA non-linear parameters which fit the measurements of FWM process. The saturation intensity is inversely proportional to the carrier lifetime; therefore higher conversion efficiency means shorter carrier lifetime. Considerably more detailed analysis shows the conversion efficiency, the ratio between the conjugate output power and the input probe power, derived in [15] from the TW equations solutions, to be expressed by:

$$\eta = \frac{|E_2(z)|^2}{|E_1(0)|^2} \tag{1}$$

where $E_2(z)$ - the conjugate mode amplitude of electric field in transverse electric mode, the output of the conjugate is proportional to the amplitude of the probe at input $E_1(0)$.

After derivation of traveling wave equations solutions and algebraic manipulations, probe and conjugate were given by:

$$E_2(z) = \exp\left[-\frac{i}{2}\alpha_I F_{\alpha_I}(z)\right] G' G^{\frac{1}{2}} E_1^*(0) \tag{2}$$

$$E_1(z) = E_1(0)\, G^{\frac{1}{2}} \exp\left[-\frac{i}{2}\alpha_I F_{\alpha_I}(z)\right] .\exp\left[-\frac{1}{2}(1 - i\alpha_I)\,\sigma F_{cd}(z, -\Omega)\right] \tag{3}$$

where; α_I is the Henry's linewidth enhancement factor, G' is the normalized conjugate output power, G is the saturated small signal gain, F_{α_I} and F_{cd} represent the contributions of Henry's linewidth enhancement factor and the carrier density modulation to the FWM response, respectively and Ω is the beating frequency. Substituting equations (A.1) to (A.8) - given in appendix A in (2) and (3), and then substituting (2) and (3) in (1) provides the result:

$$\eta = G\left|G'\right|^2 \tag{4}$$

3. SOA Characterization and Experimental Set-ups

Characterization of the SOA ASE output spectra at various bias currents is given in Fig. 2(a). The gain responses with respect to various output powers are shown in Fig. 2 (b). The SOA (Alphion

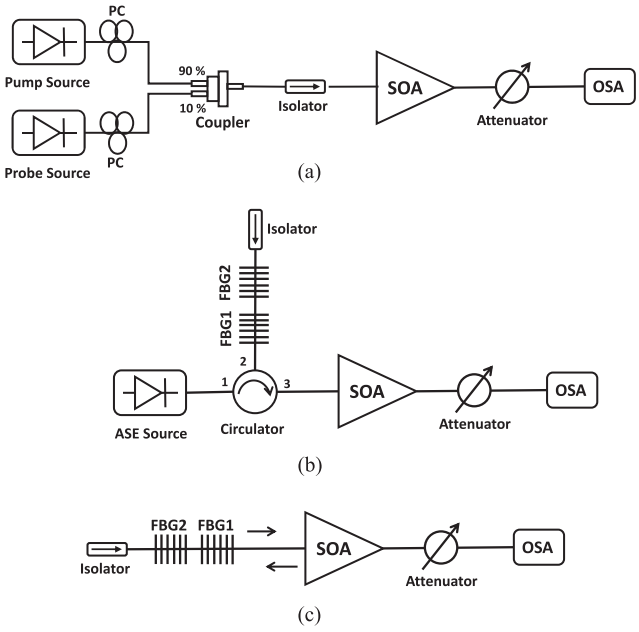

Fig. 3. Experimental set-up of (a) coherent TW FWM, (b) SS-SL TW FWM, (c) PS-SL GC FWM, in which PC: polarization controller, SOA: semiconductor optical amplifier, OSA: optical spectrum analyzer, ASE: amplified spontaneous emission, FBG: fiber Bragg grating.

SAS26p) used in the experiment has a small unsaturated gain (G_o) of 21 dB at input power of -30.2 dBm at 1548.31 nm wavelength with a saturated output power of 9.4 dBm. An optical spectrum analyzer (OSA) is used for peak-power measurements. The maximum polarization-dependent-gain between transverse electric and transverse magnetic components of the SOA-device at 550 mA-maximum operational drive current is 1.5 dB at chip temperature of 25 °C as specified in the data sheet.

Fig. 3(a) illustrates the experimental TW SOA configuration of a coherent FWM effect. Tunable laser sources were utilized as the pump and probe signals. The polarizations of both inputs were controlled carefully via two polarization controllers. The outputs were combined using a 90/10 coupler in order to control the pump-probe ratio between the FWM inputs, and sent through an isolator to prevent the backward ASE of employed SOA, which in turn served as a non-linear medium. An OSA was utilized to characterize the output of the SOA. Fig. 3(b) shows the configuration of a typical SS-SL FWM set-up. An ASE light source, with an output total ASE power of around 10.65 dBm, was used as the broadband source. Two fiber Bragg grating (FBG) filters were deployed in series, and coupled to a circulator in order to spectrally slice the pump and probe wavelengths. The 3 dB bandwidths of the filters were 0.262 nm and 0.256 nm for the 1544.41 nm probe (FBG1) and 1539.51 nm pump (FBG2) channels, respectively. Both spectrally sliced wavelengths having −13.1 dBm total output ASE power were combined at the output port of the circulator, whereby the reflected wavelengths were subsequently sent through a TW SOA. An optical isolator was used to suppress any reflection from the unfiltered ASE signal.

The experimental set-up of the proposed PS-SL FWM system based GC SOA arrangement is shown in Fig. 3(c). Two FBGs filters were attached directly at the input of SOA, as to make use of the backward ASE from SOA. The total power of backward ASE was 14.7 dBm. It was spectrally-sliced via two FBGs filters, and the resulting reflected sliced channels underwent amplifications in the SOA medium, which were manifested as backward amplified signals. These sliced channels achieved a total power of −1.3 dBm, due to the benefits associated with the backward ASE amplifications properties. The backward amplified signals were then re-injected into the SOA, so as to induce simultaneous direct interactions with the SOA medium, and all the ensuing SOA outputs were

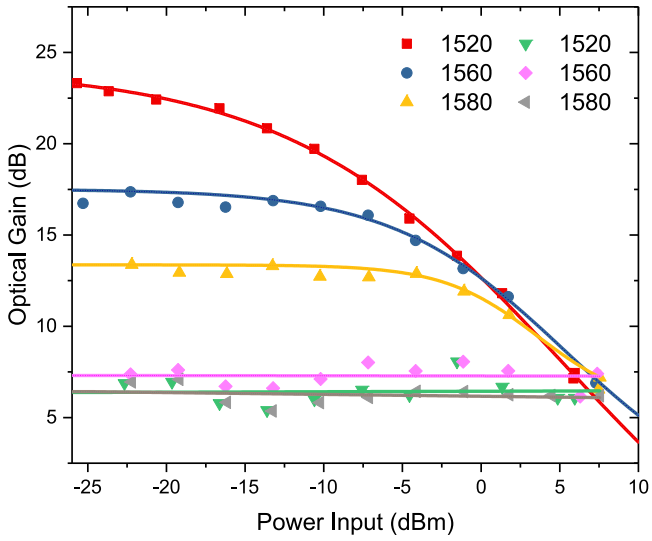

Fig. 4. Input power versus gain responses at different wavelengths in a TW configuration (red, blue, and yellow colors) and GC arrangement when a TLS is added to the proposed PS-SL set-up, in the presence of the FBGs filters, (green, purple and gray colors). The SOA bias current is 550 mA.

conveyed into the generated FWM channels. An optical isolator at the far-end input of the SOA was used to ensure unidirectional propagation for both SS-SL channels. An optical attenuator was used to attenuate the high level of output power, such that the FWM conversion efficiency could be monitored and measured via an OSA with a resolution of 0.02 nm.

In order to verify the gain clamping characteristics of the proposed PS-SL set-up, in comparison to TW configurations, a tunable laser source is added immediately before the isolator shown in Fig. 3(c), in the presence of the FBGs filters. The gain response of the SOA against the input power of laser source in a conventional TW and GC configurations at different center wavelengths (1520, 1560 and 1580 nm) are recorded in Fig. 4. The signal wavelengths are purposely selected in order to avoid overlapping with the central frequencies of the FBGs at 1539.51 and 1544.41 nm. Referring to Fig. 4, the gain for the PS-SL setup is clamped in the range of 6.0 to 7.5 dB irrespective to the input power variations, in comparison to the gain characteristics of the TW arrangement. This indicates that the SOA population inversion is fixed due to the presence of strong reflected lights by FBG1 and FBG2 [16]. This condition is also matched with the laser behavior in previous work [17].

4. Results and Discussions

The characterizations of four different FBGs filters used in the experiment, marked with red lines, are illustrated in Fig. 5(a) and (b). They were examined using an ASE source and a circulator to obtain their reflection spectra. In Fig. 5(a), FBG1 and FBG2 had center wavelengths of 1539.508 nm and 1544.409 nm, and around 34.89 dB and 34.7 dB optical signal-to-noise ratio (OSNR), respectively. The 3 dB bandwidths of the filters were 0.256 nm and 0.262 nm for the 1539.508 nm and 1544.409 nm wavelengths, respectively. The SS-SL channels at the output of the SOA, shown in blue lines, were amplified and broadened with respect to the original spectra with reduced OSNR, due to the presence of ASE in the amplification bands. SS-SL is just a simple version of a filtered ASE spectrum, and it suffers from a high filtering power loss during spectral slicing - which is compensated in the energy-efficient PS-SL through a simple laser cavity formed at the backward side of SOA. Therefore, FWM with SS-SL could not be observed with the SOA employed, due to the requirement of very high input power. While a dual-stage amplifier could be used to amplify the SS-SL channels, this will be accompanied by a high ASE level - which limits the achievement of

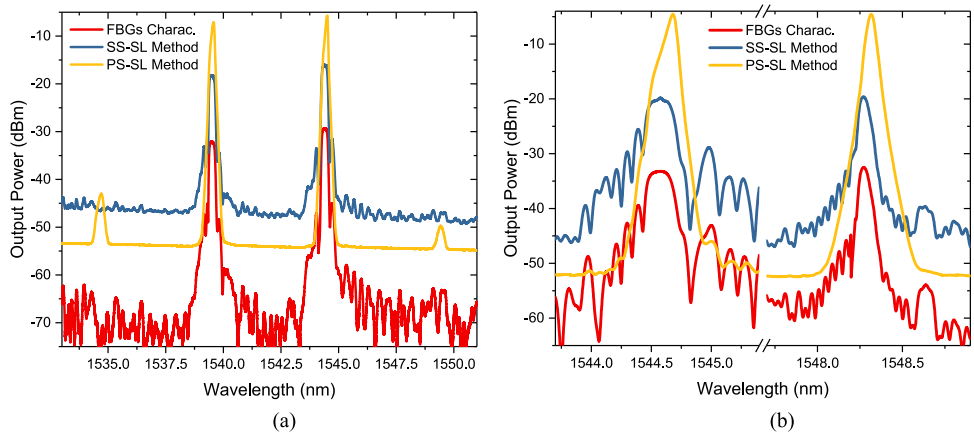

Fig. 5. The reflection spectra of four different FBGs filters (marked in red lines), SS-SL channels at the SOA output (marked in blue lines), PS-SL FWM at the output of the SOA (marked in yellow lines) compared to the reflections spectra and amplified SS-SL channels. SOA drive current: 550 mA. OSA resolution: 0.02 nm.

high peak power required to observe FWM. However, this is limited by the relatively low saturated power of SOAs, where a high input power will not be useful.

The PS-SL channels at the output of the SOA are illustrated by the yellow lines, which are compared to the original characterized channels, and also the output of the traditional SS-SL technique. The PS-SL outputs spectra were higher in OSNR values, and also narrower in bandwidth. They had spectral purities and OSNR in excess of 48.13 dB, while noise levels descended to −47.5 dBm. It is important to note that the yellow spectra shown in Fig. 5(a) had 3 dB linewidths of 0.14 nm and 0.11 nm, which were narrower than that of the spectra recorded while characterizing the FBGs filters and the conventional SS-SL outputs. The narrowing mechanism occurred due to the interference between the backward ASE and counter-propagating PS-SL patterns travelling into and out of the amplifier, which induces a transient Bragg gratings effect and dynamic modulation of the amplifier refractive index. The latter occurred due to an efficient amplifier gain saturation, which also lead to significant ASE suppression and carrier lifetime acceleration. This is supported by the GC SOA characteristics, as depicted in Fig. 4. Another example is shown in Fig. 5(b). FBG1 and FBG2 had center wavelengths of 1544.68 nm and 1548.316 nm, around 24 dB and 20.8 dB OSNR, respectively, and 0.211 nm and 0.064 nm 3 dB bandwidths, respectively. Likewise, the PS-SL output spectra were higher in OSNR values, and also narrower in bandwidths. The PS-SL outputs spectra were trimmed down to 77 pm and 49 pm for both channels, respectively. The OSNR was about 47.6 dB, while the noise level dropped to −46 dBm. The wavelength range is cut short in Fig. 5(b), in order to illustrate the narrowing mechanism accompanying the PS-SL over SS-SL method.

Fig. 6 demonstrates PS-SL FWM indicated in blue color, induced from the backward ASE of the implemented SOA associated with FBGs filters only. The spectra marked in red color are the outputs of the SOA with coherent sources. Fig. 6(a) compares between coherent FWM and PS-SL FWM. The input power was −16.91 dBm, while the bias current of the SOA was 550 mA. It is clearly seen that PS-SL inputs saturates the SOA more effectively than coherent inputs, and the ASE level of PS-SL FWM is 4.3 dB lower than that of coherent FWM. The FBG filters used had center wavelengths of 1544.68 nm and 1548.316 nm and 3 dB bandwidths of 0.211 nm and 0.064 nm, respectively. Fig. 6(b) illustrates both scenarios. The input power of coherent sources only was increased to −12.81 dBm, and the drive current of the SOA was reduced to 178 mA to purposely match both spectra on OSA ensuring an equal output power. The idler of PS-SL FWM is 7.9 dB higher in power than that of conventional FWM.

Fig. 7(a) and (b) illustrate both negative (down) and positive (up) wavelength conversions processes, respectively, using different FBGs filters than those used to present Fig. 6. Optical fiber

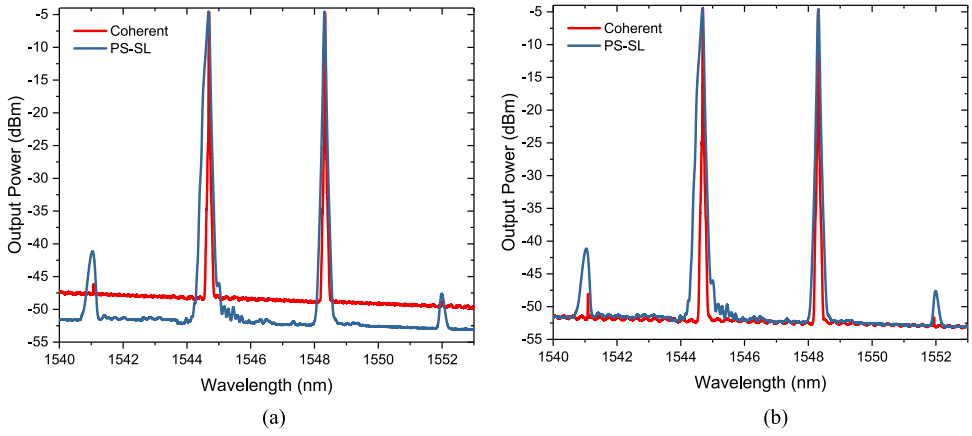

Fig. 6. Coherent FWM versus PS-SL FWM (a) input power of both coherent and PS-SL pumps: −16.91 dBm at bias current of 550 mA, (b) input power of coherent pump: −12.8 dBm at bias current of 178 mA. OSA resolution: 0.02 nm.

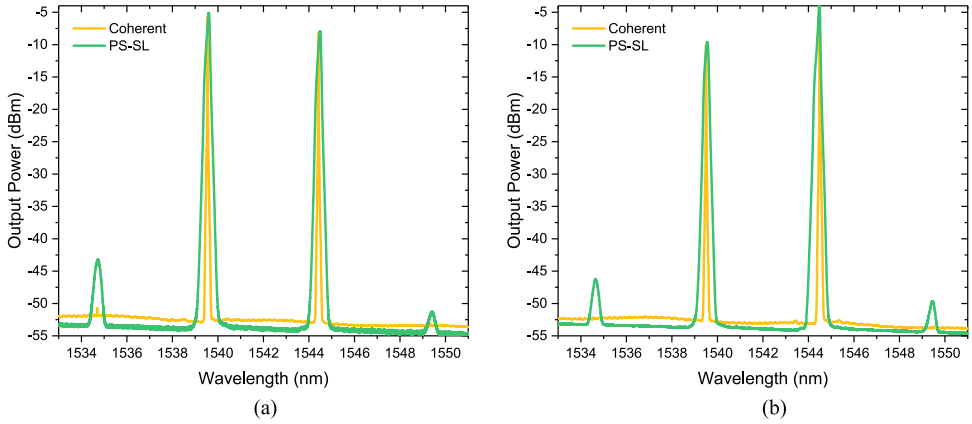

Fig. 7. Coherent FWM versus PS-SL FWM with different FBGs filters (a) negative (down) and (b) positive (up) detunings; input power of coherent pump: −12.42 dBm at bias current of 140 mA, input power of PS-SL pump: −16.2 dBm at 550 mA drive current. OSA resolution: 0.02 nm.

loops were established prior to the FBG filter responsible for probe signal generation, in order to induce an optical loss and to control the power ratio between pump and probe channels. A comparison between the FWM spectra of both PS-SL and coherent techniques is also shown in both figures. The 3 dB bandwidths of the filters used for PS-SL FWM were 0.256 nm and 0.262 nm, with 1539.51 nm and 1544.41 nm center wavelengths, respectively. The input powers of the PS-SL FWM pump and probe channels were measured to be −16.20 dBm and −19.08 dBm, respectively. These power measurements were recorded by taking the peak powers values of the pump and probe spectra on the OSA, as described in [18], [19]. The pump, probe and idler channel wavelengths were 1539.605 nm, 1544.487 nm, and 1534.726 nm, respectively. A conversion efficiency of −17.13 dB was measured across a 1544.487 nm to 1534.726 nm negative detuning. The FWM efficiency of PS-SL inputs was 8.78 dB higher than that with coherent inputs, as can be depicted from Fig. 7(a).

The maximum recorded conjugate powers (ρ) for both FWM systems, based on coherent and PS-SL inputs, are compared in Fig. 8. Tunable laser sources were used to tune the coherent inputs of FWM effects across wide conversion bandwidths. Several FBGs filters were deployed and tuned by applying strain, via a simple stage tool, in order to study the conjugate powers at different detuning spans. Blue and green lines represent theoretical conjugate powers results based

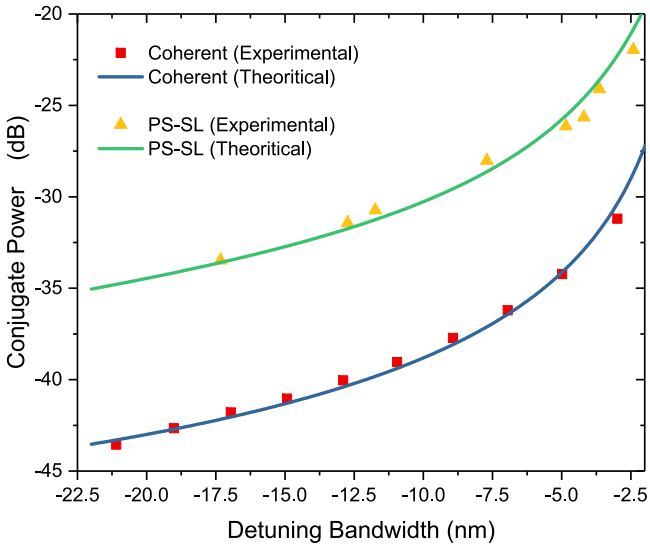

Fig. 8. Conversion bandwidth vs. conjugate power (blue line: coherent theoretical values, and red squares: coherent experimental values, green line: PS-SL theoretical values, yellow triangles: PS-SL experimental values).

TABLE 1
Non-Linear Fitting Parameters of the Implemented Semiconductor Optical Amplifier.

Symbol	Quantity	Values and Units (TW FWM)	Values and Units (GC FWM)
τ	carrier lifetime	220 ps	80 ps
τ_1	hole burning time	110 fs	50 fs
τ_2	carrier heating time	620 fs	250 fs
ε_{sh}	hole burning parameter	16x10^{-3} mW^{-1}	7.2x10^{-3} mW^{-1}
ε_{ch}	carrier heating parameter	4x10^{-3} mW^{-1}	1.8x10^{-3} mW^{-1}

on coherent and PS-SL inputs, respectively. While, red squares and yellow triangles represent practical conjugate powers of coherent and PS-SL FWM, respectively. The conjugate power (ρ) is defined as the power of the idler normalized to the output power of the probe, and given by: $\rho = |G'|^2 \exp\{Re[(1 - j\alpha_l)\sigma F_{cd}(L, -\Omega)]\}$, where; G' is found from equation A.1,α_l is the Henry's linewidth enhancement factor, σ is a proportionality constant, F_{cd} represent the contributions of carrier density modulation to the FWM response, L is the amplifier length and Ω is the beating frequency. The ρ values were calculated via computer iterations within the theoretical model defined in Appendix A with the fitting non-linear parameters detailed in Table 1. These findings applied a pump peak power of -16.20 dBm and probe peak power of -27.48 dBm, and a corresponding saturated gain (G) of 18.46 dB and 16.64 dB, obtained in the experiments for coherent and PS-SL, respectively. It was assumed that around 10% of the input power was coupled into the SOA waveguide [15].

Fig. 8 shows that an excellent match between the theory and experiment can be obtained using different material fitting parameters for coherent and PS-SL sources (see Table 1). The results confirm that the SOA implemented here showed higher efficiencies with PS-SL inputs with a faster carrier lifetime than what was attainable using coherent sources (CSs). The maximum conversion efficiency difference between both techniques is around 8.8 dB at 9.76 nm conversion bandwidth, whereas the corresponding minimum discrepancy is about 6.0 dB at detuning of -1.03 nm. This is

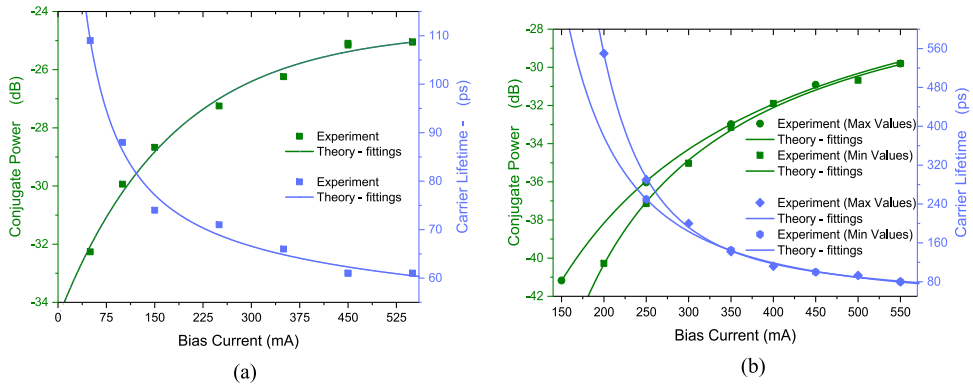

Fig. 9. (a) Bias current vs. coherent conjugate power, input pump power: +4.03 dBm, (b) bias current vs. PS-SL conjugate power, input pump power: −16.2 dBm and The detuning bandwidth is 9.76 nm and pump-probe ratio is 11.28 dB for a and b.

believed to be due to polarization matching and efficient saturation being attained at short detuning spans. With a normalized waveguide loss coefficient (α') of 0.1 used in [15], the non-linear fitting parameters with PS-SL conjugate power values obtained from the experiment were found to be as follow: $\alpha_l = 6$, $\tau = 80\,ps$, $\tau_1 = 50\,fs$, $\tau_2 = 250\,fs$, $\varepsilon_{sh.}P_s = 0.14$, $\varepsilon_{ch.}P_s = 0.035$. These terms were explained and defined earlier in the text. Noteworthy, it has been reported that Brillouin scattering impairments in optical fibers can be avoided via incoherent pumps likewise, and therefore offered better conversion efficiencies compared to coherent sources [19]–[21].

There are two factors attributed to shortening the carrier life time of the SOA in the proposed method. Firstly, the efficient saturation intensity occurring with GC SOA configuration, due to the interference between the backward ASE and counter-propagating PS-SL patterns circulating into and out of the amplifier. This induces a transient Bragg grating effect, causing a narrowing mechanism and a dynamic modulation of the amplifier refractive index. The latter occurs due to an efficient amplifier gain bleaching, which leads to carrier lifetime acceleration - as saturation intensity is inversely proportional to the carrier lifetime of the SOA. This also resulted in significant ASE suppression - in contradiction to the SS-SL technique. The PS-SL elements are trimmed down, the noise is suppressed, and can therefore theoretically be treated as coherent inputs. Another factor can be thought of in a statistical average sense; the PS-SL elements carry higher power corresponding to the numerous number of photons existed in each mode of a PS-SL channel. Every single photon within a PS-SL input channel experiences amplification. This therefore increases the optical intensity compared to coherent inputs, which leads to a higher stimulated recombination rate and therefore to a shorter carrier lifetime.

Furthermore, the proposed system performance is also examined and compared to the conventional coherent technique across wide ranges of drive currents. The drive current of the SOA was varied during both experiments. Operating SOAs at high bias currents provides larger unsaturated gain (high carrier density) - which tends to shorten their carrier life times, and consequently leads to higher FWM efficiency. As the bias current of the SOA is varied from 50 mA to 550 mA at 4.03 dBm input power, with coherent FWM inputs, the carrier lifetime is accelerated from 109 ps to 61 ps - as is depicted in Fig. 9(a). On the other hand, using PS-SL inputs at a much lower input power of −16.2 dBm and 550 mA bias current shortened the speed of the SOA from 550 ps at 200 mA down to 80 ps - in an exponential recovery trend. As can be depicted from the figures, the PS-SL conjugate power is expected to grow further in comparison to the coherent FWM trend at higher power inputs. The minimum and maximum conjugate power values shown in Fig. 9(b) are taken with different FBGs filters bandwidths. The conjugate power is also partially influenced by the available statistical powers within their differing filters bandwidths. This is also attributed to an unstable resonance of the backward ASE loop at low bias current only. It is expected that utilization of higher SOA ASE backward power will accelerate the SOA recovery time much further. Hence; the PS-SL

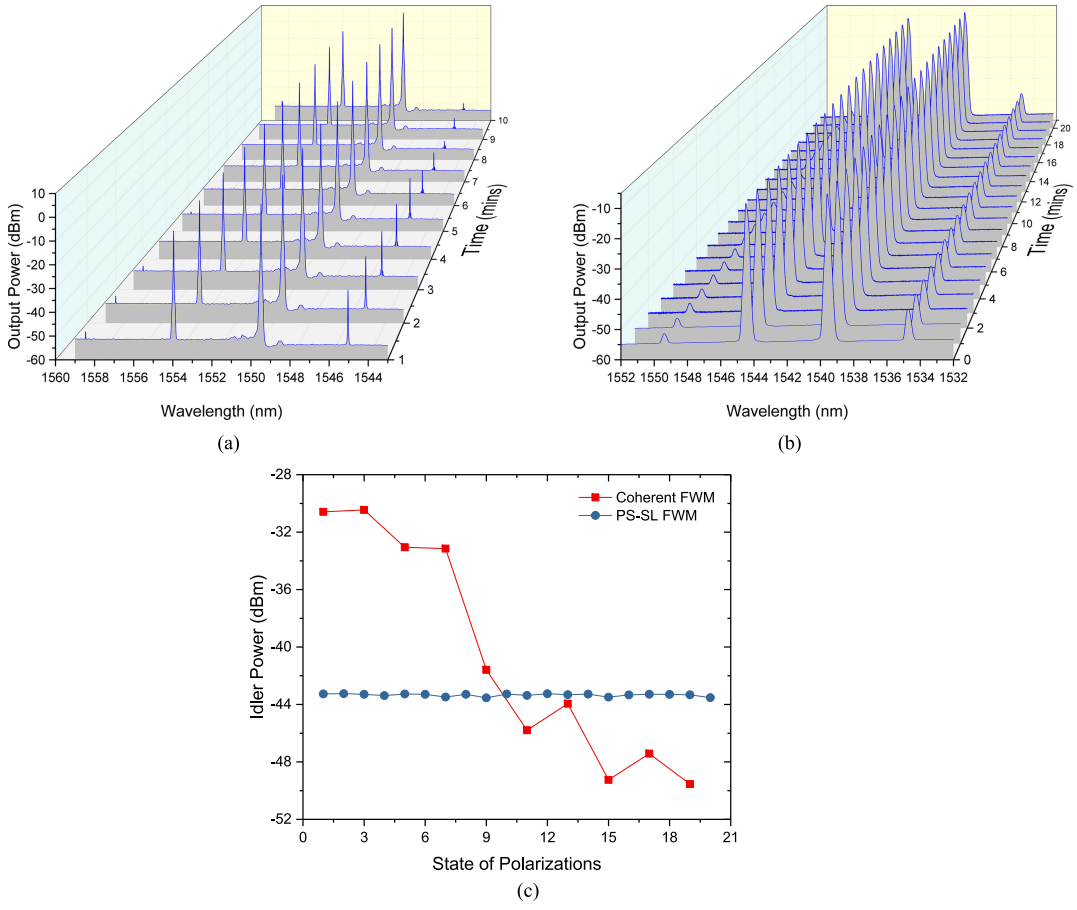

Fig. 10. (a) Polarization-dependent FWM based on coherent sources. (b) Polarization-free FWM based on PS-SL technique. (c) Idlers powers fluctuations against paddles rotations in which black and red lines represent coherent and PS-SL FWM, respectively, (Coherent and PS-SL FWM were recorded at different input powers).

method provides a more effective method to speed up the recovery of the amplifier compared to conventional coherent techniques. Bulk and QW SOAs provide relatively low unsaturated gains, saturation output powers and small-signal bandwidths, which limit their speed compared to QD and doped QW types [22]–[24]. It is expected that the proposed method would be of greater help to shorten the carrier lifetimes of doped QW and QD SOAs, owing to their higher saturation output and backward ASE powers compared to QW - which both have limited accelerated carrier lifetimes of tens of pico-seconds at low input power ranges. The proposed technique can furthermore be used for gain and nonlinearity response characterizations of all SOA types - at almost no cost and without recourse to tunable, high power and bulky coherent sources. This scheme can also be employed to produce GC multi-channels for employment in wavelength division multiplexing passive optical networks systems [12], [25]–[27].

Observation of Fig. 10(a) shows three-dimensional coherent FWM spectra using the set-up shown in Fig. 3(a), as being significantly erratic. The input power of the pump was measured to be 8.07 dBm, using an OSA with a drive current of 300 mA. The power fluctuations of the FWM components are plotted against arbitrary polarization states as a result of randomly rotating the paddles of the polarization controllers. The evaluated variations in the FWM conjugate were about 19 dB, as is clearly shown in Fig. 10(c). This was a consequence of the occurring drifting of the polarization states between pump and probe fields. Indeed without complex and costly feedback circuits, the conjugate can almost disappear [28]. On the other hand, three-dimensional PS-SL

FWM spectra which are recorded at the output of the optical attenuator in the set-up, presented in Fig. 3(c), are illustrated in Fig. 10(b), demonstrated very stable and polarization-independent features, despite slight power fluctuations in the FWM conjugates of about 0.28 dB as a maximum. This is clearly depicted from Fig. 10(c). The power input of coherent FWM is much higher than that of PS-SL FWM, showing the large idler power variations. Applying equal input power to PS-SL leads to very low idler power, and varying the polarization states will not eventually show the real variations of the FWM efficiency.

Temporal fluctuations of amplitude, phase, and polarization states on the PS-SL channels would have been equivalently transferred to the conjugate owing to the instantaneous nature of FWM mechanism. Each mode of PS-SL fields created from non-polarized backward ASE of a SOA depicted an enormous number of photons with erratically distributed states of polarizations [18], and thus is indicative of polarization matching which always takes place within spectrally-sliced incoherent paths in a statistically average sense [29]. This virtue draws attention for prospective real devices based on this configuration, since it dispenses with the need for polarization controller components.

5. Conclusion

This paper has experimentally demonstrated a new method to speed up the carrier lifetime in semiconductor optical amplifiers in a gain-clamped configuration. The experimental FWM results show that PS-SL inputs lead to higher conversion efficiencies, compared to coherent sources in a travelling-wave arrangement, and drive the SOA into the non-linear regime more quickly. The theoretical analysis has shown that the carrier lifetime was accelerated to about three times that of the speed employed with conventional coherent sources. Furthermore, FWM based on PS-SL inputs offers both an accurate polarization-independent and an economical method to characterize the non-linear parameters of a SOA.

Appendix

In this appendix, the detailed equations substituted in the conjugate mode amplitude of electric field ($E_2(z)$) and the amplitude of the probe at input $E_1(0)$ used to extract the non-linear parameters of SOA are given by:

$$G' = -\frac{1-i\alpha_l}{\alpha}\exp\left[-\frac{1}{2}\sigma F_{cd}(\Omega)\right]\sin\left[\frac{\alpha_l}{2}\sigma F_{cd}(\Omega)\right] - \frac{1}{2}\varepsilon_{sh}P_{sat}H_{sh}(\Omega)\sigma F_{sh} - \frac{1}{2}\frac{g_o}{\bar{g}}\varepsilon_{ch}P_{sat}H_{ch}(\Omega)\sigma F_{ch} \tag{A.1}$$

$$F_{cd}(\Omega) = \frac{1}{1-i\Omega\tau\alpha'}\left[\ln\left(\frac{1+\frac{GP_t(0)}{P_{sat}}-i\Omega\tau}{1+\frac{P_t(0)}{P_{sat}}-i\Omega\tau}\right)+\alpha' ln\left(\frac{G_O}{G}\right)\right] \tag{A.2}$$

$$F_{sh} = \ln\left(\frac{G_O}{G}\right) \tag{A.3}$$

$$F_{ch} = -\frac{1}{\alpha'}\left[\frac{P_t(0)}{P_{sat}}(G-1) - \ln\left(\frac{G_O}{G}\right)\right] \tag{A.4}$$

$$P_t(0) = P_{sat}\left(\frac{1-\alpha'}{\alpha'}\right)\frac{1-\left(\frac{G}{G_O}\right)^{\alpha'}}{G-\left(\frac{G}{G_O}\right)^{\alpha'}} \tag{A.5}$$

$$\sigma = \frac{P_O(0)}{P_O(0)-P_1(0)} \tag{A.6}$$

where; α' is the normalized waveguide loss coefficient, σ is a proportionality constant, F_{sh} and F_{ch} represent the contributions of spectral hole burning and carrier heating to the FWM response, respectively,P_{sat} is the saturation power, P_t is the total power input, $\bar{g}$ is the unsaturated gain coefficient, g_o is the normalization gain, ε_{sh} and ε_{ch} are the strengths of the corresponding carrier heating (CH) and spectral hole burning (SHB) non-linear effects respectively, Ω is the beating frequency, $P_O(0)$ and $P_1(0)$ are the average input powers of probe and pump elements correspondingly, τ is the spontaneous carrier lifetime, H_{ch} and H_{sh} are the Fourier transforms of the non-linear gain response due to CH and SHB respectively. These Fourier transforms are given by:

$$H_{ch}(\Omega) = \frac{1}{(1 - i\Omega\tau_1)(1 - i\Omega\tau_2)} \tag{A.7}$$

$$H_{sh}(\Omega) = \frac{1}{1 - i\Omega\tau_2} \tag{A.8}$$

where τ_1 is the characteristic time of the carrier-longitudinal optical (LO) phonon scattering that is responsible for in the cooling of the carrier distribution to the lattice temperature, and τ_2 is the characteristic time of the carrier-carrier scattering that is responsible for the filling of the hole burned by the field in the intra-band carrier distribution and also for the heating of the electron and hole gas.

References

[1] M. Li *et al.*, "Reconfigurable optical signal processing based on a distributed feedback semiconductor optical amplifier," vol. 6, 2016, Art. no. 19985.

[2] J. L. Pleumeekers *et al.*, "Acceleration of gain recovery in semiconductor optical amplifiers by optical injection near transparency wavelength," *IEEE Photon. Technol. Lett.*, vol. 14, pp. 12–14, Jan. 2002.

[3] M. A. Dupertuis *et al.*, "Extremely fast high-gain and low-current SOA by optical speed-up at transparency," *IEEE Photon. Technol. Lett.*, vol. 12, pp. 1453–1455, Nov. 2000.

[4] G. Talli and M. J. Adams, "Gain recovery acceleration in semiconductor optical amplifiers employing a holding beam," *Opt. Commun.*, vol. 245, pp. 363–370, 2005.

[5] F. Ginovart, M. Amaya, and A. Sharaiha, "Semiconductor optical amplifier studies under optical injection at the transparency wavelength in copropagative configuration," *J. Lightw. Technol.*, vol. 25, pp. 840–849, 2007.

[6] M. Sugawara *et al.*, "Recent progress in self-assembled quantum-dot optical devices for optical telecommunication: temperature-insensitive 10 Gb s −1 directly modulated lasers and 40 Gb s −1 signal-regenerative amplifiers," *J. Phys. D, Appl. Phys.*, vol. 38, pp. 2126–2134, 2005.

[7] L. Zhang *et al.*, "Reduced recovery time semiconductor optical amplifier using p-type-doped multiple quantum wells," *IEEE Photon. Technol. Lett.*, vol. 18, no. 22, pp. 2323–2325, Nov. 2006.

[8] A. J. Zilkie *et al.*, "Femtosecond gain and index dynamics in an InAs/InGaAsP quantum dot amplifier operating at 1.55 μm," *Opt. Exp.*, vol. 14, pp. 11453–11459, 2006.

[9] R. Giller, R. J. Manning, G. Talli, R. P. Webb, and M. J. Adams, "Analysis of the dimensional dependence of semiconductor optical amplifier recovery speeds," *Opt. Exp.*, vol. 15, pp. 1773–1782, 2007.

[10] F. Girardin, G. Guekos, and A. Houbavlis, "Gain recovery of bulk semiconductor optical amplifiers," *IEEE Photon. Technol. Lett.*, vol. 10, no. 6, pp. 784–786, Jun. 1998.

[11] A. M. de Melo and K. Petermann, "On the amplified spontaneous emission noise modeling of semiconductor optical amplifiers," *Opt. Commun.*, vol. 281, pp. 4598–4605, 2008.

[12] O. M. Kharraz, H. Ahmad, A. B. B. Mohammad, D. I. Forsyth, M. Dernaika, and S. W. Harun, "Performance enhancement of pre-spectrum slicing technique for wavelength conversion," *Opt. Commun.*, vol. 350, pp. 154–159, 2015.

[13] H. H. Lee, S. H. Cho, and S. S. Lee, "Efficient excess intensity noise suppression of 100-GHz spectrum-sliced WDM-PON with a narrow-bandwidth seed light source," *IEEE Photon. Technol. Lett.*, vol. 22, no. 20, pp. 1542–1544, Oct. 2010.

[14] Y.-F. Wu, C.-H. Yeh, C.-W. Chow, J.-Y. Sung, and J.-H. Chen, "Stable and wavelength-tunable self-injected reflective semiconductor optical amplifier-based fiber laser," *IEEE Photon. J.,* vol. 7, no. 4, Aug. 2015, Art. no. 1503007.

[15] A. Mecozzi, S. Scotti, A. D. Ottavi, E. Iannone, and P. Spano, "Four-wave mixing in traveling-wave semiconductor amplifiers," *IEEE J. Quantum Electron.*, vol. 31, no. 4, pp. 689–699, Apr. 1995.

[16] K. Hoin *et al.*, "A gain-clamped SOA with distributed Bragg reflectors fabricated under both ends of active waveguide with different lengths," *IEEE Photon. Technol. Lett.*, vol. 16, no. 4, pp. 999–1001, Apr. 2004.

[17] C. Michie, A. E. Kelly, I. Armstrong, I. Andonovic, and C. Tombling, "An adjustable gain-clamped semiconductor optical amplifier (AGC-SOA)," *J. Lightw.Technol.*, vol. 25, pp. 1466–1473, 2007.

[18] S. Gao, C. Yang, X. Xiao, Y. Tian, Z. You, and G. Jin, "Wavelength conversion of spectrum-sliced broadband amplified spontaneous emission light by hybrid four-wave mixing in highly nonlinear, dispersion-shifted fibers," *Opt. Exp.*, vol. 14, pp. 2873–2879 2006.

[19] Y. Tian, P. Dong, and C. Yang, "Polarization independent wavelength conversion in fibers using incoherent pumps," *Opt. Exp.*, vol. 16, pp. 5493–5498, 2008.

[20] Y. S. Jang and Y. C. Chung, "Four-wave mixing of incoherent light in a dispersion-shifted fiber using a spectrum-sliced fiber amplifier light source," in *Proc. IEEE Photon. Technol.Lett.*, 1998, vol. 10, pp. 218–220.
[21] O. M. Kharraz, A. B. B. Mohammad, D. I. Forsyth, and H. Ahmad, "Measurement of fiber non-linearity based on four-wave mixing with an ASE source," *Opt. Fiber Technol.*, vol. 32, pp. 23–29, 2016.
[22] T. Akiyama, M. Sugawara, and Y. Arakawa, "Quantum-Dot semiconductor optical amplifiers," *Proc. IEEE*, vol. 95, no. 9, pp. 1757–1766, Sep. 2007.
[23] M. Sugawara, "Recent progress in self-assembled quantum-dot optical devices for optical telecommunication: Temperature-insensitive 10 Gbs(-1) directly modulated lasers and 40 Gbs(-1) signal-regenerative amplifiers," *J. Phys. D-Appl. Phys.*, vol. 38, no. 13, pp. 2126–2134, 2005.
[24] C. Meuer *et al.*, "Cross-gain modulation and four-wave mixing for wavelength conversion in undoped and p-doped 1.3-$\mu\hbox {m} $ quantum dot semiconductor optical amplifiers," *IEEE Photon. J.*, vol. 2, no. 2, pp. 141–151, Apr. 2010.
[25] S. Kaneko, K. Jun-ichi, K. Iwatsuki, A. Ohki, M. Sugo, and S. Kamei, "Scalability of spectrum-sliced DWDM transmission and its expansion using forward error correction," *J. Lightw. Technol.*, vol. 24, pp. 1295–1301, 2006.
[26] K. Taguchi, M. Fujiwara, T. Imai, K. I. Suzuki, H. Ishii, and N. Yoshimoto, "Pattern effect suppression by injecting directly modulated synchronized gain-clamping light using inverted signal for PON application of SOA," *J. Lightw. Technol.*, vol. 32, pp. 1616–1623, 2014.
[27] R. Bonk *et al.*, "The input power dynamic range of a semiconductor optical amplifier and its relevance for access network applications," *IEEE Photon. J.*, vol. 3, no. 6, pp. 1039–1053, Dec. 2011.
[28] D. I. Forsyth and M. J. Connelly, "Dual semiconductor optical amplifier polarisation independent wavelength conversion using four-wave mixing with optoelectronic feedback," in *Proc. 17th Annu. Meet. IEEE Lasers Electro-Opt. Soc.*, 2004, vol. 1, pp. 396–397.
[29] O. M. Kharraz, A. B. B. Mohammad, D. I. Forsyth, A. A. Jasim, and H. Ahmad, "Polarization-independent ASE four-wave mixing in a fast semiconductor optical amplifier," *Opt. Commun.*, vol. 355, pp. 498–503, 2015.